Research Square

Preprints are preliminary reports that have not undergone peer review.
They should not be considered conclusive, used to inform clinical practice,
or referenced by the media as validated information.

Response timing and the cost of delay: a model-based policy counterfactual of the 2025 Foshan chikungunya outbreak in China

Tian-Yu Wang

wangty0709@hotmail.com

Guangdong Peizheng College

Research Article

Keywords: chikungunya, outbreak response, policy counterfactual, mathematical model, Aedes albopictus, surveillance, China

Posted Date: September 15th, 2026

DOI: https://doi.org/10.21203/rs.3.rs-10951988/v1

License: This work is licensed under a Creative Commons Attribution 4.0 International License.
Read Full License

Additional Declarations: No competing interests reported.

Abstract

Background

Between June and December 2025, Guangdong Province, China, experienced the largest chikungunya outbreak ever recorded in the country, with Foshan City as its epicentre. The emergency response was unprecedented in scale, but the contribution of response timing and intensity to the outcome has not been quantified. We developed a model-based policy counterfactual to ask how the outbreak would have differed under alternative response scenarios.

Methods

We coupled a weather-driven mechanistic model of *Aedes albopictus* density with a two-zone host-vector transmission model in which temperature-dependent extrinsic incubation and vector competence followed published trait surfaces. The response was encoded as a two-step schedule matching the documented timeline (case finding from 8 July 2025; citywide vector control from 19 July 2025). Parameters were estimated against post-detection-wave surveillance anchors only, with uncertainty represented by a six-start envelope. Five scenarios were compared: the fitted actual response, no response, the actual response advanced or delayed by two weeks, and a Breteau-index-triggered response.

Results

The fitted model reproduced the observed outbreak (11,988 cases; envelope 10,695 to 13,018) against approximately 10,819 officially reported for Foshan. Growth of reported cases between 15 July and 9 August 2025 was dominated by a detection wave from active case finding rather than by incidence; by 15 July true infections exceeded reported cases by a factor of 5.1 to 14.5. Removing the response gave a median of 95,182 reported cases (78,084 to 127,785), 7.9 times the fitted actual level. Advancing the response by two weeks reduced final size by 27%, a two-week delay increased it by 42%, and a Breteau-index threshold trigger reduced it by approximately half.

Conclusions

Within this reconstruction, response timing determined the scale of the 2025 Foshan outbreak more than any other single factor. Entomological thresholds were crossed weeks before the epidemic was detected, and acting on them could have substantially reduced the outbreak. The framework offers a reusable instrument for evaluating response policy in cities facing Aedes-borne outbreak risk.

Background

Chikungunya fever, a mosquito-borne viral disease caused by the chikungunya virus (CHIKV), re-emerged as a global public-health threat during the twenty-first century, with large outbreaks across Africa, Asia and the Americas [1–6]. These outbreaks were associated with substantial acute morbidity, chronic joint disease and excess mortality [7, 8]. In China, where *Aedes albopictus* is the principal vector, chikungunya has historically appeared as small, import-seeded clusters in Guangdong and neighbouring provinces [9], in a province long at the centre of dengue resurgence in China [10, 11]. That pattern changed in the summer of 2025. Following the onset of illness of an index case in Foshan City, Guangdong Province, on 16 June 2025, and the detection of a local cluster on 8 to 9 July 2025, the outbreak expanded into the largest chikungunya event ever recorded in China: by 11 November 2025 the provincial cumulative total had reached 25,258 reported cases, of which approximately 43% occurred in Foshan [12, 13], according to provincial health-authority briefings.

The public-health response was correspondingly extraordinary. A national work group was deployed to Foshan; the city was organised into response grids; door-to-door case finding and breeding-site elimination were carried out; and largescale adulticiding and larval-source management continued for months. By 20 July 2025, official briefings reported that 90% of affected villages and neighbourhoods had reduced vector density from high to medium risk or below, with one third reaching the safe level; by 9 August 2025, the compliance rate of affected villages exceeded 95%. On 26 August 2025 the city formally terminated its level-III public-health emergency response as daily new cases had remained below 50 for nine consecutive days (municipal press briefings). The door-to-door character of the campaign followed long-standing community-participation practice in *Aedes* control [14, 15], an approach whose sustained programmatic application is well documented in Singapore [16].

Two questions follow from this episode. First, what would the outbreak have looked like without this response, or with the same response shifted earlier or later in time? Second, could a response triggered directly by routine entomological surveillance, rather than by the detection of human cases, have improved the outcome? Existing work on the Foshan outbreak has estimated its transmissibility [17, 18] and characterised its viral-load dynamics [19], but the policy counterfactual, the quantitative comparison of the implemented response against plausible alternatives, has not been addressed. This question matters beyond a single outbreak: warming trends are extending the season and geographic range of *Aedes*-borne transmission [20–23], temperate-region outbreaks have already demonstrated that *Ae. albopictus* can sustain epidemic transmission at the margins of the range [24], and cities at those margins will face the same decision, of when and how hard to respond, under increasing time pressure.

Here we developed a model-based policy counterfactual of the 2025 Foshan outbreak. The framework couples a weather-driven mechanistic model of vector density with a two-zone host-vector transmission model whose temperature-dependent traits follow published laboratory surfaces, and calibrates the vector-control response to the officially documented response timeline. All epidemic quantities are produced by simulation; the study involves no human participants and uses only publicly reported aggregate data.

Methods

Study overview

The framework has three layers. A weather-driven density model produces the response-adjusted Breteau index (BI) of each zone from ERA5 reanalysis weather. A host-vector transmission model converts vector abundance into human infections through temperature-dependent trait surfaces. A response layer encodes the documented vector-control timeline as explicit intervention schedules, which are varied across counterfactual scenarios. The model was calibrated to officially reported quantities (case-curve anchors, citywide BI values and response-coverage milestones) and evaluated with a multi-start envelope that propagates parameter uncertainty into all reported outcomes. The analysis workflow is outlined in Fig. 1.

Data and outbreak anchors

Daily ERA5 reanalysis weather for Foshan (mean, maximum and minimum temperature; precipitation; relative humidity) from 1 January 2024 to 31 August 2026 was obtained through the Open-Meteo archive [25]. Outbreak anchors were compiled from national and provincial health-authority briefings and the published literature and are summarised in Table 1. The response timeline was quantified from official briefings: on 20 July 2025, 90% of affected villages had reduced vector density from high to medium risk or below and 33% had reached the safe level; on 28 July 2025, 78% of affected villages were at the safe level; on 5 August 2025, the mean vector indices of the core affected communities in Lecong town were 1.1 (mosquito density) and 1.8 (BI); and by 9 August 2025 the compliance rate of affected villages exceeded 95%. Level-III emergency response was terminated on 26 August 2025 after nine consecutive days with fewer than 50 daily new cases.

Table 1
Outbreak anchors and response milestones used for model calibration and validation

Date / period	Quantity	Value	Source type
2025-06-16	Index-case onset	1 case	Municipal briefing
2025-07-08 / 09	Local cluster detected (Shunde)	—	Municipal briefing
2025-07-15	Cumulative cases, Shunde	478	Municipal briefing
2025-07-19	Cumulative cases, citywide	1873	Municipal briefing
2025-07-19	Daily new cases (peak)	674	Municipal briefing
2025-07-20	Affected villages below high risk / safe	90% / 33%	Municipal briefing
2025-07-26	Cumulative cases, province / Foshan	4824 / 4754	Provincial briefing
2025-07-28	Affected villages at safe level	78%	Xinhua News Agency
2025-08-05	Lecong town core villages, mosquito / BI	1.1 / 1.8	Nanfang Daily
2025-08-09	Affected-village compliance rate	> 95%	Municipal briefing
2025-08-26	Level-III response terminated	< 50 daily cases for 9 days	Municipal briefing
2025-11-11	Provincial cumulative total	25258 (Foshan 42.92%)	Provincial briefing
2025 (Jul / Aug)	Citywide mean BI	8.5 / 6.2	Municipal CDC via media
2026-03	Citywide mean MOI	1.04 (748 stations)	Municipal CDC via media

Weather-driven density model

Weekly vector density was generated by a mechanistic potential-fecundity-index (PFI) model parameterised from published laboratory studies of *Ae. albopictus* [26]. Weekly development rate followed a Briere function of temperature [27] with lower and upper thresholds of 10 C and 39 C; adult survival followed a Gaussian function of temperature with a maximum of 0.95 at 27 C, modulated by relative humidity; and a saturating rainfall factor captured breeding-site availability, following rainfall- and temperature-driven abundance models for this species [28] and the container-breeding ecology of urban *Aedes* [29]. Weekly values were interpolated to daily resolution and scaled by a fitted calibration constant, and the citywide BI was modelled as the response-adjusted product of this baseline and two protection stocks representing source reduction and space spraying. Protection stocks accumulate with

weekly onset lag and exponential decay under repeated coverage; the aggregate decay constants (0.45 and 0.30 per week) encode the citywide rebound described in official communications, whereby untreated sites are re-colonised within two to three weeks. Citywide BI anchors were used as soft validation targets: the fitted configuration reproduces the July and August 2025 citywide means (8.5 and 6.2) and remains consistent with the low winter/spring values observed in 2026 municipal reporting and with a historical district-level May reference of 12.18 from Chancheng District in 2016.

Two-zone host-vector model

The city was represented as two zones: the hot-spot zone (Shunde District, which concentrated 92.96% of reported cases during the early explosion) and the remainder of the city. Each zone carries an independent copy of a host-vector compartment model of the class used in previous chikungunya studies [30–32], extended with an asymptomatic human compartment following the Foshan transmission study [17], comprising susceptible, exposed, symptomatic-infectious, asymptomatic-infectious and recovered human compartments, and susceptible, exposed and infectious vector compartments. Human latent and incubation periods were fixed at 7 days, the symptomatic and asymptomatic infectious periods at 8 days, the asymptomatic fraction at 0.140, and vertical transmission in the vector at 0.168, following the values used in that study [17]. The vector extrinsic incubation period was made temperature-dependent following the trait surface of Tegar et al. [33], interpolated between 8.74 days at 18 C and 1.74 days at 30 C, consistent with the experimentally characterised temperature dependence of arbovirus extrinsic incubation [34] and with the vector competence of *Ae. albopictus* for CHIKV [35], and a refinement over the fixed incubation periods used in previous work. Vector abundance in each zone was imposed from the response-adjusted density trajectory of that zone, so that each response scenario implies its own vector population and hence its own transmission intensity. Case reporting was modelled as the symptomatic onset stream multiplied by an ascertainment process that rises with detection effort; the detection surge associated with the expansion of nucleic-acid testing to 35 hospitals and door-to-door fever screening from 20 July 2025 is an explicitly documented component of the response.

Response encoding and counterfactual arms

The documented response was encoded as a two-step schedule. Step one, at the detection date (8 July 2025), activates case finding and isolation, represented by an isolation factor that reduces the human-to-vector transmission force and by an ascertainment step. Step two, at the citywide campaign (19 to 20 July 2025), raises vector-control coverage to its fitted peak, combining the source-reduction and adult-control modalities whose effectiveness has been evaluated in previous campaigns [36, 37], with the hot-spot zone escalating first and the remaining districts following with a fitted stagger. After the termination of level-III response on 26 August 2025, coverage settles to a normalised sustaining level. The escalation offset and the zone stagger were fitted jointly with the transmission parameters. Five scenarios were compared: (i) the fitted actual response; (ii) no response; (iii) the actual response advanced by two

weeks; (iv) the actual response delayed by two weeks; and (v) a threshold-triggered response that begins when the simulated no-response BI first exceeds the national transmission-risk threshold of 5 [38], an action level whose epidemiological rationale in larval-index surveillance has been evaluated previously [39–42]. Scenario (v) represents a response driven directly by routine entomological surveillance rather than by human-case detection.

Calibration and uncertainty

Because reported cases during the explosive phase of mid-July to early August were strongly shaped by the detection surge (see Results), a decoupling of reported counts from incidence documented in other major arbovirus and respiratory outbreaks [43, 44], the calibration window excluded this transition and used the post-saturation anchors from 16 August 2025 onwards, when ascertainment had stabilised (13 cumulative anchors, with the ascertainment fraction effectively 1). Parameters (the two transmission coefficients, the initial seed, the density calibration constants of the two zones, the response coverage peaks, the escalation offset, the zone stagger, the isolation floor and the baseline ascertainment fraction) were estimated by Nelder-Mead optimisation over six multi-start configurations; the spread across converged fits is reported as the uncertainty envelope of every model-based quantity. Because the number of free parameters is comparable to the number of post-wave anchors, absolute parameter identification is not achievable, and the across-start spread, rather than any single point estimate, is the honest representation of uncertainty.

Ethics statement

The study used only publicly reported aggregate surveillance data and computer simulation; no human participants, individual-level data or biological samples were involved.

Large language model assistance (Kimi K3, Moonshot AI) was used for code development and debugging and for language editing; every script was executed by the author and all code, numerical outputs and text were reviewed and verified by the author.

Results

The reconstruction of the observed outbreak, the detection-wave decomposition and the counterfactual comparison are presented in turn (Figs. 2, 3 and 4).

The outbreak and its documented response

The outbreak is summarised in Table 1. Reported cases accumulated slowly for the first month (the provincial total for the week of 8 to 14 July was 481) and then rose explosively: the citywide cumulative total reached 1,873 on 19 July, 4,754 on 26 July and 7,524 by 2 August, with 92.96% of early cases concentrated in Shunde District. Daily new cases peaked at 674 on 19 July. The response escalated in

step: the citywide campaign began in the week of 19 July, and the officially quantified response milestones (90% of affected villages below high risk by 20 July, 78% at the safe level by 28 July, and above 95% compliance by 9 August) bracket the inflection of the curve. Level-III response was terminated on 26 August 2025, and provincial weekly additions fell to single digits by late November.

The detection wave: reported cases decoupled from incidence

Reported cases are a product of incidence and ascertainment, and the two processes separated sharply in this outbreak (Fig. 2). For the first four weeks, reported growth was slow, consistent with low baseline detection. From 15 July onwards, reported cases rose far faster than any biologically plausible incidence trajectory: the interval from 15 to 26 July alone contributed more than 3,700 reported cases. This jump coincided with the documented expansion of detection capacity (nucleic-acid testing extended to 35 additional hospitals and door-to-door fever screening across tens of thousands of households), which is part of the response itself. After early August, once detection was saturated, reported and true curves re-joined.

Two conclusions follow. First, models fitted naively to the raw early reported curve conflate incidence with ascertainment, and transmissibility estimates from such fits inherit that confounding. Second, the early phase of the outbreak was substantially larger than the reported counts suggest. Back-extrapolating the calibrated model to 15 July 2025 yields a median estimate of approximately 3,000 true infections across the city against 478 officially reported cases, an under-ascertainment factor of 6.4 at the central fit, with a multi-start envelope of 5.1 to 14.5 (Fig. 4a). In other words, by the time the outbreak was detected, transmission had been established for weeks and the true seed population was already an order of magnitude larger than the reported count.

Model reconstruction of the actual outbreak

The fitted actual-response scenario reproduced the observed outbreak within the multi-start envelope (Fig. 2): the final reconstructed total was 11,988 reported cases (envelope 10,695 to 13,018) against approximately 10,819 officially reported for Foshan, and the model tracked the post-wave plateau, in which daily additions fell below 50 by late August and the cumulative curve flattened through the autumn as the response transitioned to a sustaining regime and temperatures declined.

Counterfactual scenarios

Table 2 and Fig. 3 report the five scenarios. Without any response, the median reconstructed outbreak reached 95,182 reported cases (envelope 78,084 to 127,785), 7.9 times the fitted actual level; under the constant baseline ascertainment of the no-response scenario this corresponds to a cumulative true burden on the order of six hundred thousand infections, an attack rate of approximately 6% of the population, within the range observed in previous large chikungunya outbreaks in immunologically naive populations [4]. Advancing the response by two weeks reduced the median final size to 8,746 cases, a reduction of 27% relative to the actual response; delaying it by two weeks increased the median final size

to 17,037 cases, an increase of 42%. A response triggered by the national entomological threshold (BI > 5) began several weeks before the human outbreak was detected, because simulated vector density crossed the threshold in early summer long before any case was reported, and reduced the median final size to 6,306 cases, approximately half of the actual level.

Table 2
Counterfactual outcomes by response scenario (multi-start envelope over six converged fits)

Scenario	Final reported cases, median	Envelope	Ratio vs actual	Cases averted vs actual, median
No response	95182	78084–127785	7.94	−83194 (more cases)
Response 2 weeks later	17037	14156–18736	1.42	−5049 (more cases)
Actual response (fitted)	11988	10695–13018	1.00	reference
Response 2 weeks earlier	8746	7366–9651	0.73	+ 3242 (fewer cases)
BI-threshold trigger (BI > 5)	6306	3720–6980	0.53	+ 5682 (fewer cases)

Reported cases under each scenario are computed under the surveillance regime implied by that scenario (the no-response scenario retains baseline detection throughout). Ratios compare medians across the six multi-start fits.

The asymmetry between the early and late scenarios reflects the mechanics of the season: because vector density was still rising through June and July, an earlier response suppressed the population while it had not yet peaked, whereas a delayed response confronted a larger vector population at its seasonal maximum. All scenario orderings were preserved across every multi-start fit.

Vector-density validation

The response-adjusted BI trajectories of the two zones remained consistent with all available surveillance anchors (Fig. 4b): the hot-spot zone peaked above the citywide July mean, the citywide means matched the reported 8.5 and 6.2 for July and August, the simulated density was below the risk threshold during the winter and early spring of 2026 in line with the municipal report of a March 2026 mean MOI of 1.04, and the historical district-level May reference from 2016 falls within the simulated no-response summer range.

Discussion

Principal findings

In a model-based reconstruction of the largest chikungunya outbreak recorded in China, the response, and above all its timing, dominated the outcome. The implemented response, for all its scale, was still an after-the-fact response: it began the week the outbreak was detected, roughly three weeks after the index onset and at least several weeks after simulated vector density had crossed the national risk threshold. The counterfactual analysis indicates that the response averted approximately seven-eighths of the potential reported burden relative to no response, that a two-week advance would have prevented roughly a quarter of all cases, that a two-week delay would have expanded the outbreak by more than 40%, and that a response triggered directly by routine entomological surveillance could have halved the outbreak without waiting for human cases.

The detection wave as a methodological caution

The decomposition in Fig. 2 carries a methodological message for outbreak modelling in general. During the explosive phase, reported cases were driven primarily by the expansion of detection capacity that accompanies the response itself: testing was extended, house-to-house screening was conducted, and case ascertainment rose towards saturation. Models fitted to the raw reported curve over this window therefore estimate a hybrid of incidence and ascertainment. This concern applies to the Foshan outbreak specifically: the present reconstruction, calibrated only outside the detection-wave window, implies that true infections by mid-July exceeded reported cases several-fold. Transmissibility estimates from the early reported curve should accordingly be interpreted as joint properties of the epidemic and the response-driven detection process. More broadly, any outbreak met with a surge of case finding will exhibit this decoupling [43, 44], and reconstruction efforts should either model ascertainment explicitly or calibrate outside the surge window.

Timing, thresholds and the value of entomological surveillance

The counterfactual asymmetry, in which a two-week delay costs more than a two-week advance saves, reflects the rising density through the early summer: the later the response, the larger the vector population it confronts at its seasonal peak. The threshold-triggered scenario quantifies the alternative: the national surveillance framework already defines BI > 5 as the action level, and simulated density crossed that level weeks before the first human case was detected. A response governed by this routine entomological signal would have begun during the build-up phase rather than after the epidemic was established, and its advantage over the actual response persisted across all multi-start fits. This is consistent with the broader outbreak-control literature: the speed of detection and response is a primary determinant of controllability [45], containment windows contract rapidly with delay [46, 47], model-based evaluations of control measures in the temperate Italian setting support rapid response [48], quantified counterfactuals of intervention timing during the COVID-19 pandemic reached the same conclusion at national scale [49], and the gap between outbreak detection and response has been documented as a systemic weakness of surveillance-triggered control programmes [50]. It also reflects the ecology of the vector, since sustained pressure is required because *Ae. albopictus* rebounds rapidly

after suppression [51]. This supports the view that the binding constraint on outbreak control in *Aedes*-endemic cities is not the intensity of the response but the trigger for initiating it.

The September shift as observational context

After Foshan terminated its emergency response in late August, the provincial epicentre shifted to Jiangmen, which reported thousands of weekly cases through September and October while Foshan fell to tens. This observational contrast, in a neighbouring city within the same season, is consistent with the modelled conclusion that sustained vector-control pressure holds transmission near the threshold while its absence allows explosive growth. It cannot serve as a controlled comparison, since the cities differ in demography, environment and seeding history, but it illustrates the stakes of the same policy choice made by neighbouring municipalities in the same month.

Limitations

Several limitations qualify these findings. First, all results are simulation-based; the model reconstructs and compares scenarios within a calibrated mathematical system and makes no claim to reproduce unobserved events exactly. Second, the vector density calibration rests on sparse citywide anchors (the July and August 2025 means, both response-affected, and winter values from 2026 reporting), because monthly citywide BI means were not published for 2024 or for most of 2025; the density scale is therefore an inferred quantity, bounded by a historical district-level reference, and its uncertainty is propagated through the multi-start envelope rather than eliminated. Third, the citywide aggregate response encoding summarises what was in reality a spatially heterogeneous campaign concentrated in the affected villages; the fitted coverage peaks should be read as citywide averages of a much more focal effort. Fourth, the ascertainment process is represented as a step coupled to the response, whereas the true detection process was certainly smoother; the under-ascertainment estimate is a model-dependent point range rather than a measurement; post-outbreak serosurveys, when available, would independently bound this quantity [52]. Fifth, the two-zone structure abstracts from within-district heterogeneity and human mobility. Sixth, the framework does not model healthcare capacity, behaviour or economics. Finally, the counterfactual outcomes are relative quantities conditioned on the fitted system; they are intended to rank response scenarios, not to forecast absolute case counts for future events.

Implications

For cities at the margins of the expanding *Aedes* range, three operational conclusions follow. First, the entomological surveillance infrastructure that already exists in most endemic cities contains the trigger information; the model indicates that responding to it, rather than waiting for human cases, is worth approximately half an outbreak. Second, response timing dominates response scale: the difference between acting two weeks earlier and two weeks later was comparable to the entire difference between the actual response and doing nothing at all. Third, reconstruction frameworks of the kind developed here, in the tradition of model-based policy evaluation [53] and consistent with the integrated approach of the global vector control response [54], can be pre-positioned: once weather data and a response log

are available, the counterfactual questions that will inevitably be asked after the event can be answered while the policy decisions are still being made.

Conclusions

Within a weather-driven, two-zone reconstruction of the 2025 Foshan chikungunya outbreak, the officially documented response averted the large majority of the potential reported burden, response timing carried consequences comparable to the response itself, and a trigger based on the routine entomological threshold would have begun control weeks before human-case detection. Reported cases during the explosive phase were dominated by a response-driven detection wave, and early true incidence exceeded reported counts several-fold. As warming extends the season and range of *Aedes*-borne transmission, cities should treat entomological thresholds, not human-case counts, as the operational trigger for outbreak response.

Abbreviations

BI
Breteau index
CHIKV
chikungunya virus
EIP
extrinsic incubation period
ERA5
fifth-generation ECMWF reanalysis
PFI
potential fecundity index
MOI
mosquito-ovitrap index.

Declarations

Ethics approval and consent to participate.

Not applicable. This study is entirely simulation-based and used only publicly reported aggregate surveillance data; no human participants, individual-level data or animals were involved.

Trial registration.

Clinical trial number: not applicable.

Consent for publication.

Not applicable. The manuscript contains no identifiable individual data.

Competing interests.

The author declares no competing interests.

Funding.

This research received no specific funding.

Author Contribution

T.-Y. Wang: Conceptualization, Methodology, Software, Formal analysis, Investigation, Data curation, Visualization, Writing – original draft, Writing – review & editing.

Acknowledgements.

Not applicable.

Declaration on the use of generative AI. During the preparation of this work the author used Kimi K3 (Moonshot AI) for code development and language editing. The author reviewed and edited all AI-generated content and takes full responsibility for the integrity and accuracy of the publication.

Data Availability

All model code, the compiled anchor database with source references for every quantitative claim, and the scripts reproducing all figures and tables are openly available at https://github.com/GustaveKateb0709/foshan-chikungunya-counterfactual and archived at Zenodo (https://doi.org/10.5281/zenodo.22530930). ERA5 reanalysis data were obtained through the Open-Meteo archive (https://open-meteo.com/).

References

1. Pialoux G, Gaüzère BA, Jauréguiberry S, et al. Chikungunya, an epidemic arbovirosis. Lancet Infect Dis. 2007;7(5):319–27. 10.1016/S1473-3099(07)70107-X.
2. Burt FJ, Rolph MS, Rulli NE, et al. Chikungunya: a re-emerging virus. Lancet. 2012;379(9816):662–71. 10.1016/S0140-6736(11)60281-X.

3. Weaver SC, Lecuit M. Chikungunya virus and the global spread of a mosquito-borne disease. N Engl J Med. 2015;372(13):1231–9. 10.1056/NEJMra1406035.
4. Renault P, Solet JL, Sissoko D, et al. A major epidemic of chikungunya virus infection on Réunion Island, France, 2005–2006. Am J Trop Med Hyg. 2007;77(4):727–31. 10.4269/ajtmh.2007.77.727.
5. Morrison TE. Reemergence of chikungunya virus. J Virol. 2014;88(20):11644–7. 10.1128/JVI.01432-14.
6. Yactayo S, Staples JE, Millot V, et al. Epidemiology of chikungunya in the Americas. J Infect Dis. 2016;214(suppl 5):S441–5. 10.1093/infdis/jiw390.
7. Schilte C, Staikovsky F, Couderc T, et al. Chikungunya virus-associated long-term arthralgia: a 36-month prospective longitudinal study. PLoS Negl Trop Dis. 2013;7(3):e2137. 10.1371/journal.pntd.0002137.
8. Mavalankar D, Shastri P, Bandyopadhyay T, et al. Increased mortality rate associated with chikungunya epidemic, Ahmedabad, India. Emerg Infect Dis. 2008;14(3):412–5. 10.3201/eid1403.070720.
9. Wu D, Wu J, Zhang Q, et al. Chikungunya outbreak in Guangdong Province, China, 2010. Emerg Infect Dis. 2012;18(3):493–5. 10.3201/eid1803.110034.
10. Lai S, Huang Z, Zhou H, et al. The changing epidemiology of dengue in China, 1990–2014: a descriptive analysis of 25 years of nationwide surveillance data. BMC Med. 2015;13:100. 10.1186/s12916-015-0336-1.
11. Jing Q, Wang M, Tang X, et al. Data informed analysis of 2014 dengue fever outbreak in Guangzhou: impact of multiple environmental factors and vector control. J Theor Biol. 2017;416:161–79. 10.1016/j.jtbi.2016.12.014.
12. Li Y, Jiang S, Zhang M, et al. An outbreak of chikungunya fever in Foshan City, Guangdong Province, China, July 2025. China CDC Wkly. 2025;7(32):1064–5. 10.46234/ccdcw2025.172.
13. Gong W, Wang D, Chen Q, et al. Outbreak of chikungunya virus with Aedes albopictus-adaptive mutations, Guangdong Province, China, 2025. China CDC Wkly. 2025;7(49):1528–32. 10.46234/ccdcw2025.260.
14. Gubler DJ, Clark GG. Community involvement in the control of Aedes aegypti. Acta Trop. 1996;61(2):169–79. 10.1016/0001-706X(95)00103-L.
15. Heintze C, Garrido MV, Kroeger A. What do community-based dengue control programmes achieve? A systematic review of published evaluations. Trans R Soc Trop Med Hyg. 2007;101(4):317–25. 10.1016/j.trstmh.2006.08.007.
16. Ooi EE, Goh KT, Gubler DJ. Dengue prevention and 35 years of vector control in Singapore. Emerg Infect Dis. 2006;12(6):887–93. 10.3201/eid1206.051210.
17. Zhao Y, Li J, Zhao Z, et al. Estimating the transmissibility of the 2025 chikungunya fever outbreak in Foshan, China: a modelling study. Infect Dis Poverty. 2025;14:106. 10.1186/s40249-025-01376-8.

18. Luo M, Sun J. Chikungunya outbreak in Guangdong Province, China, 2025. Infect Med. 2025;4(3):100200. 10.1016/j.imj.2025.100200.
19. Wan S, Zhang X, Cong X, et al. Viral load dynamics of chikungunya virus in human specimens — Foshan City, Guangdong Province, China, 2025. China CDC Wkly. 2025;7(33):1067–72. 10.46234/ccdcw2025.182.
20. Kraemer MUG, Sinka ME, Duda KA, et al. The global distribution of the arbovirus vectors Aedes aegypti and Ae. albopictus. eLife. 2015;4:e08347. 10.7554/eLife.08347.
21. Mordecai EA, Cohen JM, Evans MV, et al. Detecting the impact of temperature on transmission of Zika, dengue, and chikungunya using mechanistic models. PLoS Negl Trop Dis. 2017;11(4):e0005568. 10.1371/journal.pntd.0005568.
22. Liu-Helmersson J, Quam M, Wilder-Smith A, et al. Climate change and Aedes vectors: 21st century projections for dengue transmission in Europe. EBioMedicine. 2016;7:267–77. 10.1016/j.ebiom.2016.03.046.
23. Colón-González FJ, Sewe MO, Tompkins AM, et al. Projecting the risk of mosquito-borne diseases in a warmer and more populated world: a multi-model, multi-scenario intercomparison modelling study. Lancet Planet Health. 2021;5(7):e404–14. 10.1016/S2542-5196(21)00132-7.
24. Rezza G, Nicoletti L, Angelini R, et al. Infection with chikungunya virus in Italy: an outbreak in a temperate region. Lancet. 2007;370(9602):1840–6. 10.1016/S0140-6736(07)61779-6.
25. Hersbach H, Bell B, Berrisford P, et al. The ERA5 global reanalysis. Q J R Meteorol Soc. 2020;146(730):1999–2049. 10.1002/qj.3803.
26. Delatte H, Gimonneau G, Triboire A, et al. Influence of temperature on immature development, survival, longevity, fecundity, and gonotrophic cycles of Aedes albopictus, vector of chikungunya and dengue in the Indian Ocean. J Med Entomol. 2009;46(1):33–41. 10.1603/033.046.0105.
27. Briere JF, Pracros P, Le Roux AY, et al. A novel rate model of temperature-dependent development for arthropods. Environ Entomol. 1999;28(1):22–9. 10.1093/ee/28.1.22.
28. Tran A, L'Ambert G, Lacour G, et al. A rainfall- and temperature-driven abundance model for Aedes albopictus populations. Int J Environ Res Public Health. 2013;10(5):1698–719. 10.3390/ijerph10051698.
29. Zahouli JBZ, Koudou BG, Müller P, et al. Urbanization is a main driver for the larval ecology of Aedes mosquitoes in arbovirus-endemic settings in south-eastern Côte d'Ivoire. PLoS Negl Trop Dis. 2017;11(7):e0005751. 10.1371/journal.pntd.0005751.
30. Dumont Y, Chiroleu F, Domerg C. On a temporal model for the Chikungunya disease: modeling, theory and numerics. Math Biosci. 2008;213(1):80–91. 10.1016/j.mbs.2008.02.008.
31. Yakob L, Clements ACA. A mathematical model of chikungunya dynamics and control: the major epidemic on Réunion Island. PLoS ONE. 2013;8(3):e57448. 10.1371/journal.pone.0057448.
32. Manore CA, Hickmann KS, Xu S, et al. Comparing dengue and chikungunya emergence and endemic transmission in A. aegypti and A. albopictus. J Theor Biol. 2014;356:174–91. 10.1016/j.jtbi.2014.04.033.

33. Tegar S, Brass DP, Purse BV, et al. Temperature-sensitive incubation, transmissibility and risk of Aedes albopictus-borne chikungunya virus in Europe. J R Soc Interface. 2026;23(235):20250707. 10.1098/rsif.2025.0707.
34. Watts DM, Burke DS, Harrison BA, et al. Effect of temperature on the vector efficiency of Aedes aegypti for dengue 2 virus. Am J Trop Med Hyg. 1987;36(1):143–52. 10.4269/ajtmh.1987.36.143.
35. Vazeille M, Moutailler L, Coudrier D, et al. Two chikungunya isolates from the outbreak of La Réunion (Indian Ocean) exhibit different patterns of infection in the mosquito, Aedes albopictus. PLoS ONE. 2007;2(11):e1168. 10.1371/journal.pone.0001168.
36. Esu E, Lenhart A, Smith L, et al. Effectiveness of peridomestic space spraying with insecticide on dengue transmission; systematic review. Trop Med Int Health. 2010;15(5):619–31. 10.1111/j.1365-3156.2010.02489.x.
37. Bowman LR, Donegan S, McCall PJ. Is dengue vector control deficient in effectiveness or evidence? Systematic review and meta-analysis. PLoS Negl Trop Dis. 2016;10(3):e0004551. 10.1371/journal.pntd.0004551.
38. Chinese Center for Disease Control and Prevention. Guideline for dengue prevention and control (2014 edition) [in Chinese]. Beijing: Chinese Center for Disease Control and Prevention; 2014.
39. Focks DA, Chadee DD. Pupal survey: an epidemiologically significant surveillance method for Aedes aegypti: an example using data from Trinidad. Am J Trop Med Hyg. 1997;56(2):159–67. 10.4269/ajtmh.1997.56.159.
40. Sánchez L, Vanlerberghe V, Alfonso L, et al. Aedes aegypti larval indices and risk for dengue epidemics. Emerg Infect Dis. 2006;12(5):800–6. 10.3201/eid1205.050866.
41. Runge-Ranzinger S, McCall PJ, Kroeger A, et al. Dengue disease surveillance: an updated systematic literature review. Trop Med Int Health. 2014;19(9):1116–60. 10.1111/tmi.12333.
42. Aryaprema VS, Xue RD. Breteau index as a promising early warning signal for dengue fever outbreaks in the Colombo District, Sri Lanka. Acta Trop. 2019;199:105155. 10.1016/j.actatropica.2019.105155.
43. Bhatt S, Gething PW, Brady OJ, et al. The global distribution and burden of dengue. Nature. 2013;496(7446):504–7. 10.1038/nature12060.
44. Li R, Pei S, Chen B, et al. Substantial undocumented infection facilitates the rapid dissemination of novel coronavirus (SARS-CoV-2). Science. 2020;368(6490):489–93. 10.1126/science.abb3221.
45. Fraser C, Riley S, Anderson RM, et al. Factors that make an infectious disease outbreak controllable. Proc Natl Acad Sci USA. 2004;101(16):6146–51. 10.1073/pnas.0307506101.
46. Ferguson NM, Cummings DAT, Cauchemez S, et al. Strategies for containing an emerging influenza pandemic in Southeast Asia. Nature. 2005;437(7056):209–14. 10.1038/nature04017.
47. Peak CM, Childs LM, Grad YH, et al. Comparing nonpharmaceutical interventions for containing emerging epidemics. Proc Natl Acad Sci USA. 2017;114(15):4023–8. 10.1073/pnas.1616438114.

48. Poletti P, Messeri G, Ajelli M, et al. Transmission potential of chikungunya virus and control measures: the case of Italy. PLoS ONE. 2011;6(5):e18860. 10.1371/journal.pone.0018860.
49. Lai S, Ruktanonchai NW, Zhou L, et al. Effect of non-pharmaceutical interventions to contain COVID-19 in China. Nature. 2020;585(7825):410–3. 10.1038/s41586-020-2293-x.
50. Harrington J, Kroeger A, Runge-Ranzinger S, et al. Detecting and responding to a dengue outbreak: evaluation of existing strategies in country outbreak response planning. J Trop Med. 2013;2013:756832. 10.1155/2013/756832.
51. Zheng B, Yu J, Xi Z, et al. The annual abundance of dengue and Zika vector Aedes albopictus and its stubbornness to suppression. Ecol Model. 2018;387:38–48. 10.1016/j.ecolmodel.2018.09.004.
52. Sissoko D, Moendandze A, Malvy D, et al. Seroprevalence and risk factors of chikungunya virus infection in Mayotte, Indian Ocean, 2005–2006: a population-based survey. PLoS ONE. 2008;3(8):e3066. 10.1371/journal.pone.0003066.
53. Halloran ME, Ferguson NM, Eubank S, et al. Modeling targeted layered containment of an influenza pandemic in the United States. Proc Natl Acad Sci USA. 2008;105(12):4639–44. 10.1073/pnas.0706849105.
54. World Health Organization. Global vector control response 2017–2030. Geneva: World Health Organization; 2017.

Figures

Fig. 1. Study workflow.

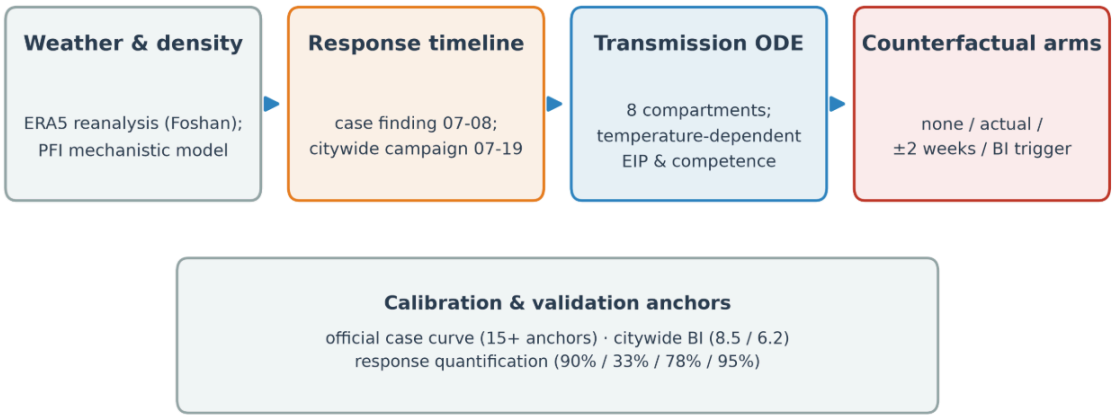


Figure 1

Study workflow and counterfactual design. ERA5 reanalysis weather drives a literature-anchored mechanistic density model; the officially documented two-step response timeline is encoded as explicit

intervention schedules; a two-zone host-vector transmission model converts vector abundance into human infections; five response scenarios are compared against the calibration and validation anchors.

Fig. 1. Study workflow.

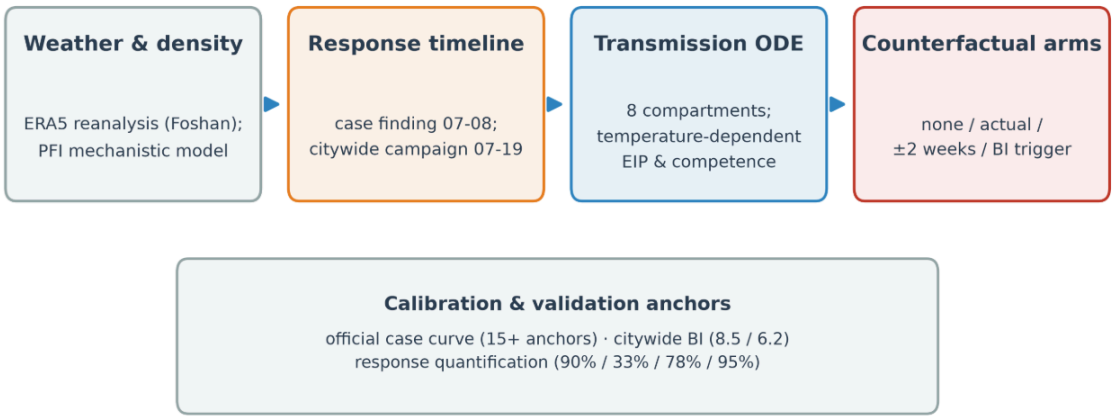


Figure 1

Study workflow and counterfactual design. ERA5 reanalysis weather drives a literature-anchored mechanistic density model; the officially documented two-step response timeline is encoded as explicit intervention schedules; a two-zone host-vector transmission model converts vector abundance into human infections; five response scenarios are compared against the calibration and validation anchors.

Fig. 2. Reported cases, model reconstruction and the detection wave.

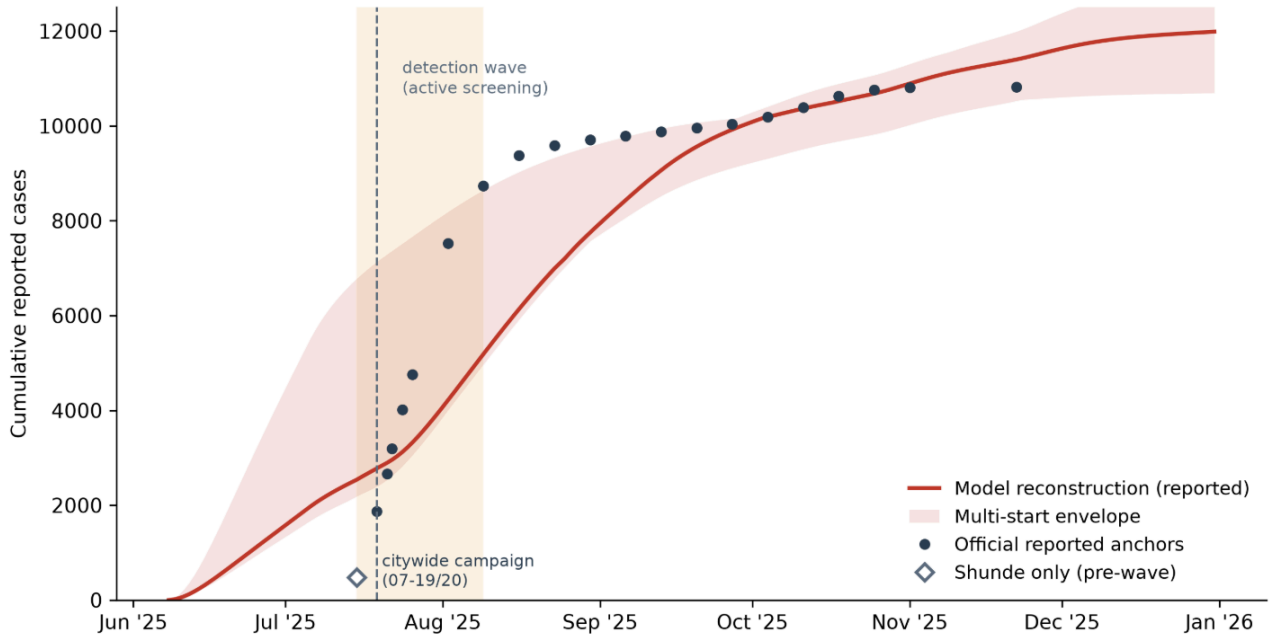


Figure 2

Reported cases, model reconstruction and the detection wave. Observed cumulative reported cases (points), the fitted actual-response reconstruction (line) and its multi-start envelope (band). The shaded window marks the detection wave (15 July to 9 August 2025), during which reported cases were dominated by the expansion of case finding rather than by incidence; the dashed line marks the start of the citywide campaign (19 to 20 July).

Fig. 2. Reported cases, model reconstruction and the detection wave.

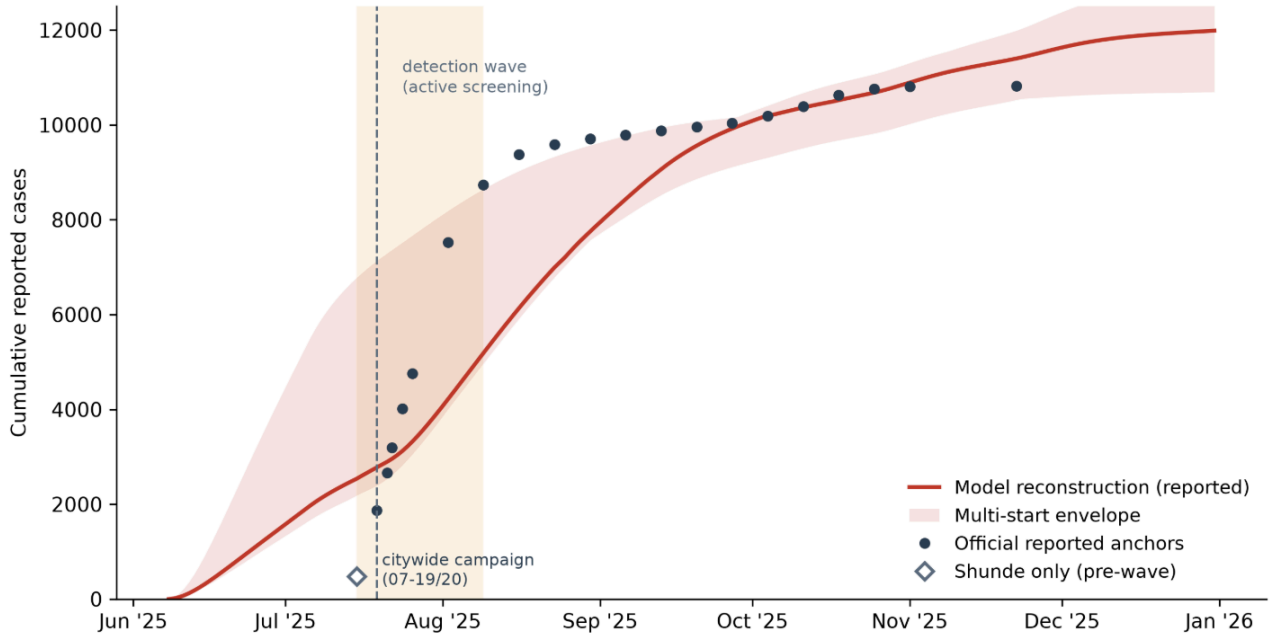


Figure 2

Reported cases, model reconstruction and the detection wave. Observed cumulative reported cases (points), the fitted actual-response reconstruction (line) and its multi-start envelope (band). The shaded window marks the detection wave (15 July to 9 August 2025), during which reported cases were dominated by the expansion of case finding rather than by incidence; the dashed line marks the start of the citywide campaign (19 to 20 July).

Fig. 3. Counterfactual reported-case trajectories under five response scenarios.

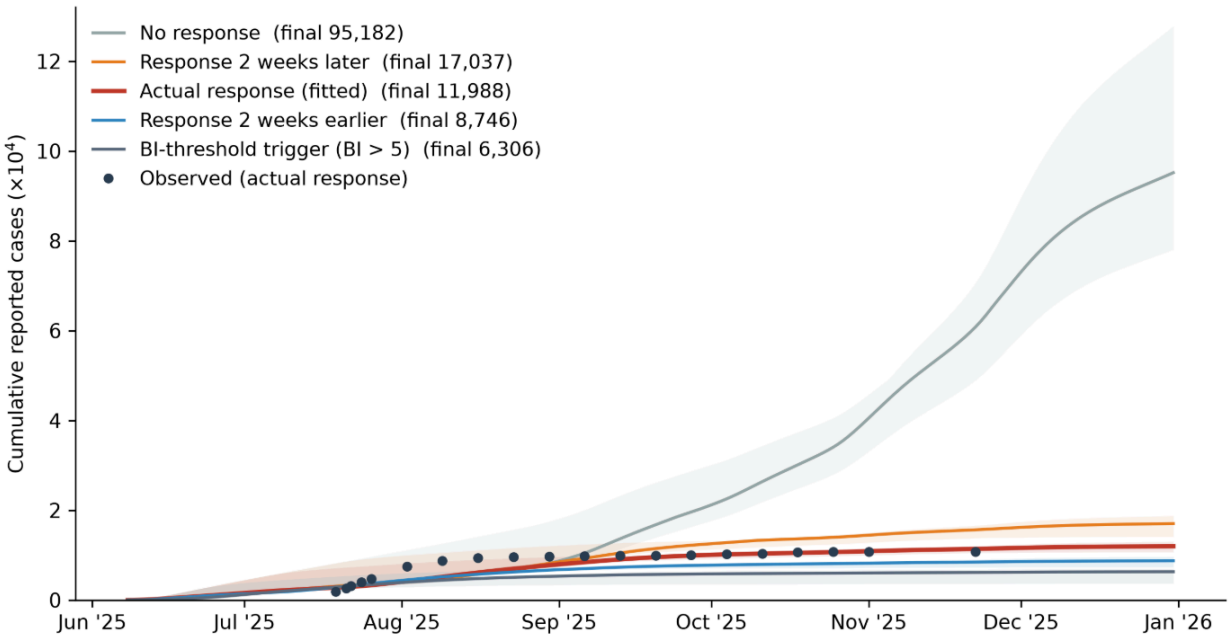


Figure 3

Counterfactual reported-case trajectories under five response scenarios. Median citywide reported-cumulative curves for the no-response, delayed (two weeks), fitted actual, advanced (two weeks) and BI-threshold-triggered scenarios, with multi-start envelopes (bands) and observed anchors (points). Final sizes are given in the legend.

Fig. 3. Counterfactual reported-case trajectories under five response scenarios.

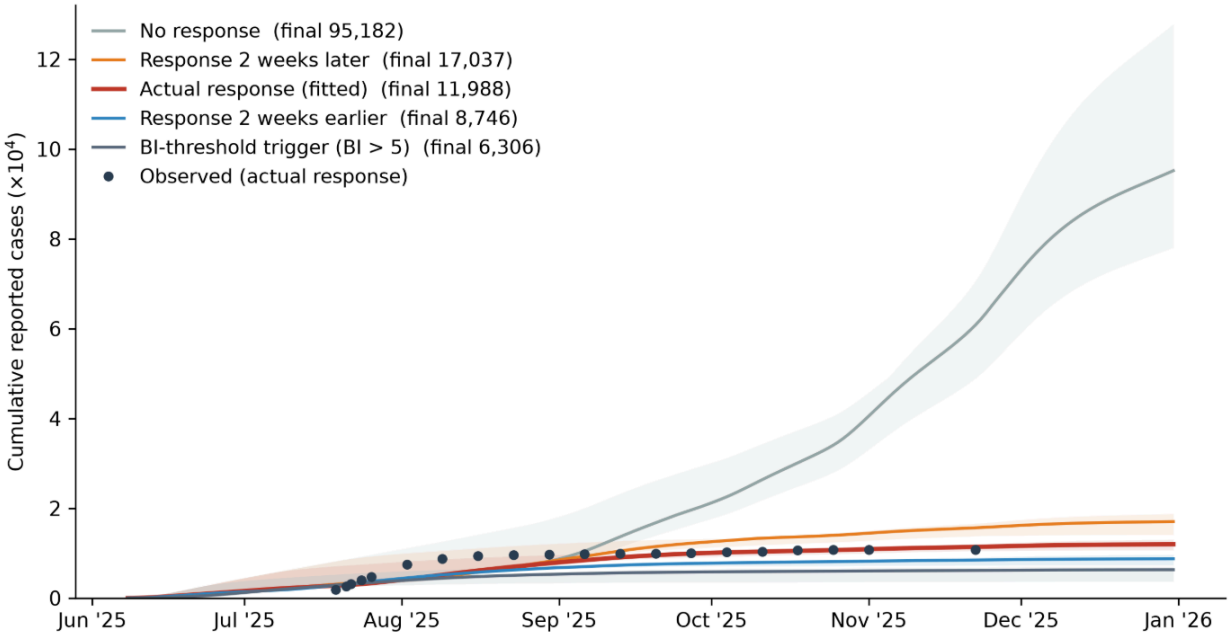
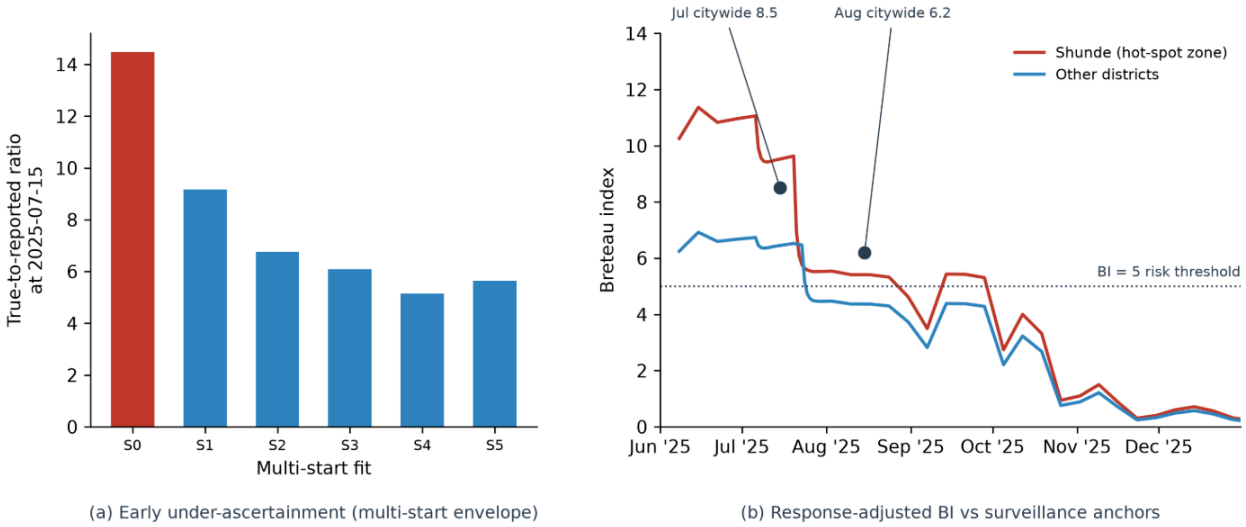


Figure 3

Counterfactual reported-case trajectories under five response scenarios. Median citywide reported-cumulative curves for the no-response, delayed (two weeks), fitted actual, advanced (two weeks) and BI-threshold-triggered scenarios, with multi-start envelopes (bands) and observed anchors (points). Final sizes are given in the legend.

Fig. 4. Under-ascertainment envelope and density-model validation.



(a) Early under-ascertainment (multi-start envelope)

(b) Response-adjusted BI vs surveillance anchors

Figure 4

Under-ascertainment envelope and density-model validation. (a) Ratio of model-reconstructed true infections to reported cases on 15 July 2025 across the six multi-start fits; all fits exceed 5. (b) Response-adjusted BI trajectories of the two zones against surveillance anchors: the July and August 2025 citywide means (8.5 and 6.2), the March 2026 municipal MOI (1.04, outside the plotted window), and the national risk threshold (BI = 5).

Fig. 4. Under-ascertainment envelope and density-model validation.

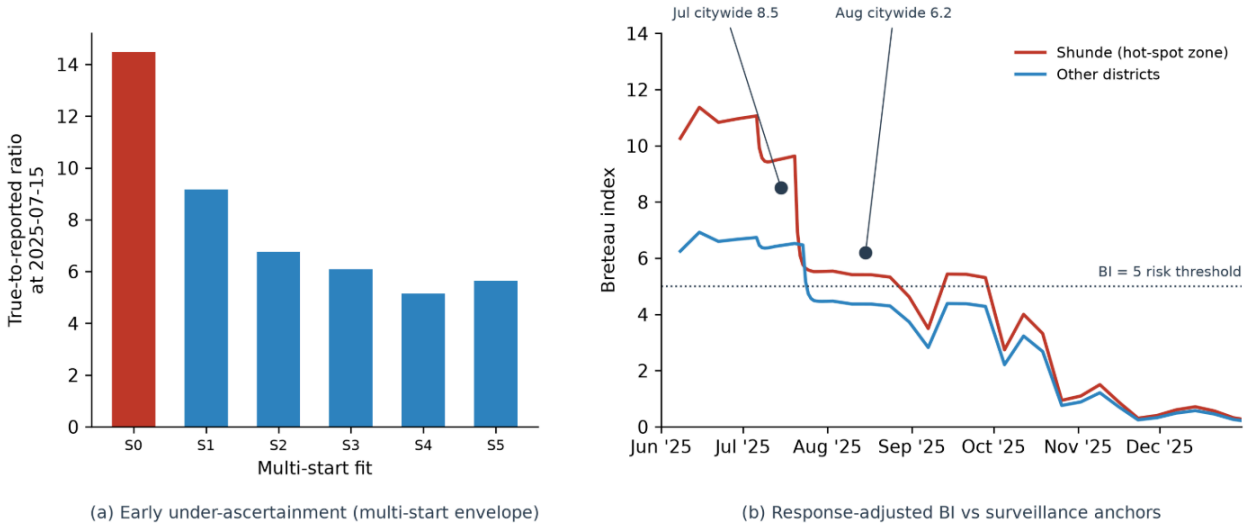


Figure 4

Under-ascertainment envelope and density-model validation. (a) Ratio of model-reconstructed true infections to reported cases on 15 July 2025 across the six multi-start fits; all fits exceed 5. (b) Response-adjusted BI trajectories of the two zones against surveillance anchors: the July and August 2025 citywide means (8.5 and 6.2), the March 2026 municipal MOI (1.04, outside the plotted window), and the national risk threshold (BI = 5).